Change Detection Based on SAR Images

I.Cathrine Ruffina., M.E.,/ECE
Mrs.M.Jeyalakshmi, AP/ECE
SSM Institute of Engineering &Technology, Dindigul

Abstract: Change detection of remote sensing images quantitatively analyzes image information at different times in the same area, so as to obtain the change information of the coverage area . Synthetic aperture radar (SAR) is an active remote sensing technology that can collect ground information at any time and under any conditions. The explicit solution of the traditional methods has the disadvantages of unstable results and requiring many iterations. To solve the problem, a new method, lag ratio and saliency map combined detection, is proposed in this work and applied to change detections of synthetic aperture radar (SAR) images. The saliency-guided GGMM is capable of capturing the primary pixel-based change information and handling highly imbalanced datasets. The whole process chain is automatic with an efficient computation. The proposed approach was validated MATLAB environment.

I. INTRODUCTION

The ability of synthetic aperture radar to detect flooding beneath a plant canopy has been demonstrated for a wide variety of herbaceous and woody vegetation types. The potential exists to conduct accurate regional surveys of seasonal flooding events, independent of cloud cover, for input to hydrological and biogeochemical models. On a smaller scale, accurate wetlands delineation would be of great value to managers of forest, wildlife, and fisheries resources. In order to realize the potential for operational mapping of inundation, robust classification methods are needed which do not require repeated optimization by scene or date. The accuracy of traditional parametric classifiers (e.g., maximum likelihood) is likely to be compromised by sceneto-scene variability in absolute sensor calibration, dielectric constant of soil and vegetation, phenological state of vegetation, and vegetation community structure. Knowledge-based expert systems offer an alternative approach using classification rules derived from a spectral knowledge base. We illustrate here how tree-based models can be used to construct classification rules from a microwave spectral database and to select optimal sets of sensor parameters for mapping of inundation in the floodplain and estuary of the Altamaha River, Georgia.

The rest of the paper is organized as follows. Section II gives a brief overview of work related method. Section III and IV describes the preliminaries and the proposed methodology. Section V presents the experimental results obtained from the proposed method and comparison with existing work. The paper is Conclusion insection VI respectively.

II. RELATED WORKS

Biswajeet Pradhan et al [1] proposed anefficient methodology to recognize and mapflooded areas by using TerraSAR-X imagery.Biswajeet Pradhan et al [2] is proposed to identify flooded areas using multitemporal RADARSAT-2 imageries.Lisa Landuyt et al [3] is presented an in-depth assessment and comparison of the established pixel-based flood mapping approaches, including global and enhanced thresholding, active contour modeling and change detection. The methods were tested on medium-resolution SAR images of different flood events and lakes across the U.K. and Ireland and were evaluated on both accuracy and robustness. Corneliu Octavian Dumitru et al [4] present data analytics for a quantitative analysis in a rapid mapping scenario applied for damage assessment of the 2013 floods in Germany and the 2011 tsunami in Japan. Giorgio Boni et al [5] is presented the prototype system and describes in detail the near real-time flood mapping algorithm implemented in the system. The algorithm was previously developed to classify CSK images, and is modified here in order to be applied to S-1 data too.Marian Mierla et al [6] is used to generate the hydrological risk map of floods within the fluvial delta, cartographic materials created by predecessors and LiDAR techniques were used.

III. PRELIMINARIES

Lisa Landuyt et al [7] presented an in-depth assessment and comparison of the established pixelbased flood mapping approaches, including global and enhanced thresholding, active contour modeling and change detection. The methods were tested on medium-resolution SAR images of different flood events and lakes across the U.K. and Ireland and were evaluated on both accuracy and robustness. Results indicate that the most suited method depends on the area of interest and its characteristics as well as the intended use of the observation product. Due to its high robustness and good performance, tiled thresholding is suited for automated, nearreal time flood detection and monitoring. Active

contour models can provide higher accuracies but require long computation times that strongly increase with increasing image sizes, making them more appropriate for accurate flood mapping in smaller areas of interest.

A number of established flood mapping approaches has been selected for assessment and comparison. An overview of the selected methods is provided. In this section, each of these methods is described in more detail.

A. Global Thresholding

Thresholding is an efficient and probably the simplest approach for image binarization. Assuming the presence of two pixel classes with substantially different pixel distributions, a threshold value is determined to classify the image. An overview of existing algorithms is provided by Sezgin and Sankur. In this paper, four widely applied algorithms are selected.

The Otsu algorithm determines an optimum threshold based on the maximization of the between-class variance of the foreground (flooded) and background (nonflooded) pixels in the image. This between-class variance can be calculated as follows:

$$\sigma_B^2 = \omega_f \omega_b (\mu_f - \mu_b)^2 \quad (1)$$

where, μf and μb are the mean intensity of the foreground and background pixels, respectively. ωf and ωb denote the respective class fractions. Although widely applied, this algorithm relies on some important assumptions. The class density functions are assumed Gaussian and both the class sizes and variances should be similar. When these assumptions are violated, the optimal threshold tends to split the class of the larger size or variance. Moreover, a skewed density function or the presence of outliers will cause a bias in the calculated class means [28]. The Otsu algorithm has been used for SAR-based flood mapping in several studies.

Kittler and Illingworth (KI) addressed the threshold optimization problem as a minimum-error Gaussian density fitting problem. The optimum threshold is determined based on the minimization of a cost function J that reflects the amount of overlap between the Gaussian density functions of the foreground and background classes.

The Minimum Cross Entropy algorithm solves the threshold optimization problem by minimizing the cross entropy between the original and the classified images, without any *a priori* assumptions regarding the class distributions.

The algorithm developed by Yen *et al.* also makes use of the entropy. Whereas Li and Lee aim at minimizing the cross-entropy between the input gray-level image and the segmented image, this algorithm aims at maximizing the correlation contributed by the foreground and background classes.

IV PROPOSED SYSTEM

In this paper, a two-step automatic change detection chain for rapid flood mapping based on Sentinel-1 Synthetic Aperture Radar (SAR) data is presented. First, a reference image is selected from a set of potential image candidates via a Jensen-Shannon (JS) divergence-based index. Second, saliency detection is applied on log-ratio data to derive the prior probabilities of changed and unchanged classes for initializing the following expectation maximization (EM) based generalized Gaussian mixture model (GGMM). The saliency-guided GGMM is capable of capturing the primary pixel-based change information and handling highly imbalanced datasets. A fully connected conditional random field (FCRF) model, which takes long-range pairwise potential connections into account, is integrated to remove the ambiguities of the saliency-guided GGMM and to achieve the final change map. The whole process chain is automatic with an efficient computation.

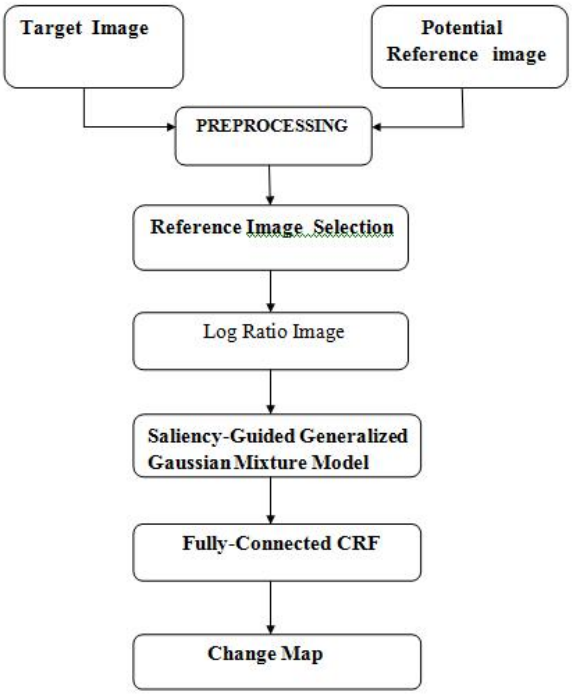

Fig. 4.1 proposed block diagram

4.1 Reference image index

The reference image selection process consists of two steps. Firstly, some potential image candidates are collected from the Copernicus Open Access Hub, which should fulfill the following criteria: the data should be acquired from the same relative orbit and with the same polarization configuration as the flood image. Especially in regions with pronounced seasonal flooding, only images acquired in the same period of the year as the target image should be collected (Hostache et al., 2012). Secondly, the final reference image is selected from the collected images based on the reference index (describe later in this section). The optimal candidate should be acquired during a period without flood (noted as "non-flooded") and should represent the "normal behavior" of the scene. It is worth to mention that too many collected potential candidates could be time-consuming with the corresponding preprocessing and increase the storage burden as well, a too small volume of candidates will degrade the optimization of the final reference image. Considering the high temporal resolution (12 days for a single satellite and 6 days for the constellation of two satellites) of Sentinel-1 data and the systematic global acquisition plan of the satellite mission, it can be assumed that images acquired during the latest year prior to the flood could be a proper potential candidate set.

KL divergence (Kullback and Leibler, 1951) is one of the most widely used similarity measures for image comparison in many application fields, such as image retrieval (Choy and Tong, 2010), image quantitative evaluation (Pheng et al., 2016), change detection (Cui et al., 2016). Suppose $pX(x)$ and $pY(x)$ are the densities of random variables X and Y, respectively, the KL divergence from X to Y is given by

$$K(X|Y) = \int \log\left(\frac{p_X(x)}{p_Y(x)}\right) p_X(x)dx \quad (2)$$

$K(X\ Y)$ has a value ≥ 0 and it is small when two pdfs are close to each other. When KL divergence is performed on local similarity measures like in a sliding window, which is generally used in change detection, one parametric SAR image model could be used to make the KL divergence analytically tractable with a closed-form expression (Cui et al., 2016). It is not valid to use a single statistic model for global similarity measure between two SAR images over large areas as they are heterogeneous with different land cover types. Here, the empirical distribution function is used to substitute the pdf in computing KL divergence.

Saliency-guided generalized Gaussian mixture model

The log-ratio operator between the flood image and the reference image as shown in Eq. (3) is used in this paper as Bujor et al. (2004) pointed out that the ratio operator is proper to detect sharp changes like those associated with flood areas.

$$X_{lr} = \log\left(\frac{X_{flood}}{X_{ref}}\right) \quad (3)$$

*Xref*is the reference image selected by the reference index. The log-ratio image *Xlr*is scaled to 256 possible gray-level values in the range [0, 255] for the subsequent analysis. We can take the pdf $p(x)$ of the log-ratio image *Xlr*as a mixture of two probability density functions associated with the changed (flooded) and unchanged (non-flooded) components.

Fully-connected conditional random field

CRF is a popular discriminative model for modeling spatial information of images in computer vision tasks (Quattoni et al., 2007; Rabinovich et al., 2007; Torralba et al., 2004). In contrast to the traditional local-range CRF models, which consider contextual information in the neighborhood, the recently proposed fully-connected CRF (Philipp and Koltun, 2011) establishes pairwise potentials on all pair of pixels in the image, refining pixel-based classification significantly.

IV. SIMULATION RESULTS

In this section, the simulation results are implemented using MATLAB2014 which is figured in 5.1,5.2,5.3 and the performance graphs are figured in 5.5 and fig 5.6

Image 1

STEP 1: Preprocessing

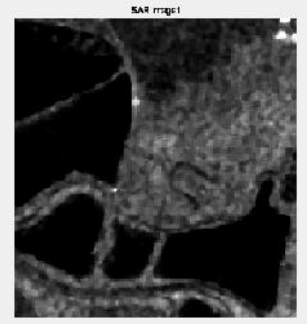

Fig 5.1 SAR Image Before Flood

STEP 2: To read the image

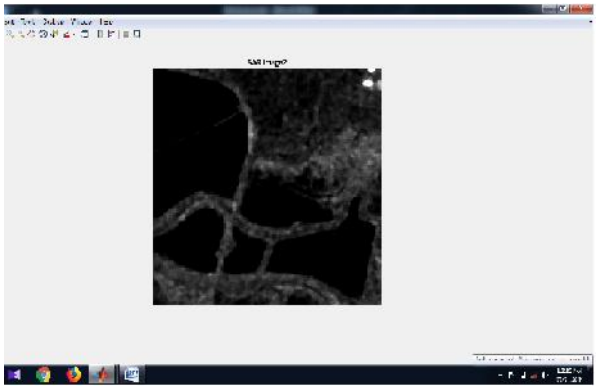

Fig 5.2 SAR Image After Flood

STEP 3: Log-Ratio Image

Fig 5.3 Log Ratio Image

Output image

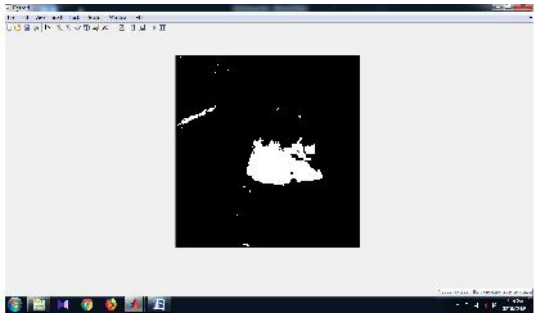

Fig 5.4 Final Image

Image 2

STEP 1: Preprocessing

Fig 5.5 SAR Image Before Flood

STEP 2: To read the image

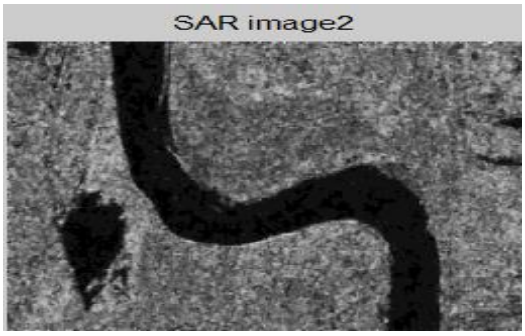

Fig 5.6 SAR Image After Flood

STEP 3: Log-Ratio Image

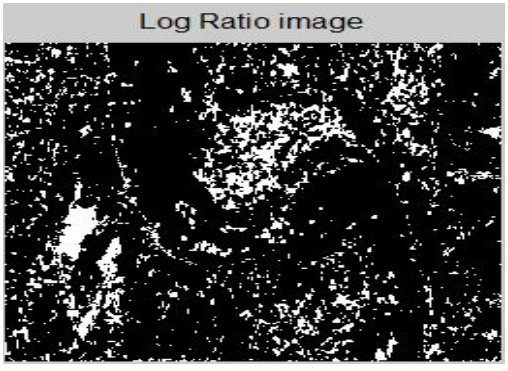

Fig 5.7 Log Ratio Image

Output image

Fig 5.8 Final Image

GRAPH 1: FALSE NEGATIVE

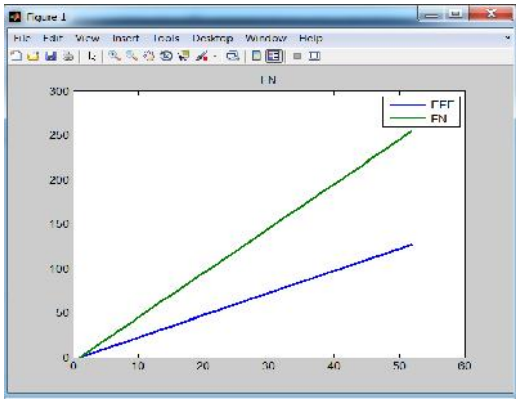

5.9 Graph on False Negative

GRAPH 2: FALSE POSITIVE

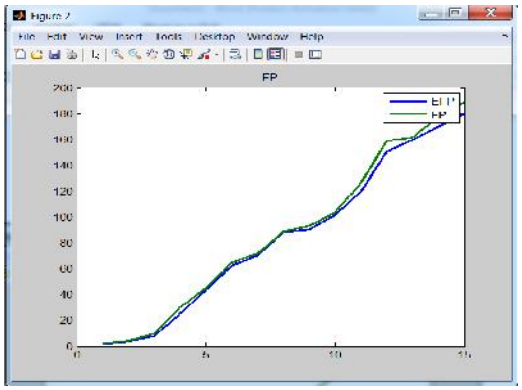

Figure 5.10 Graph on False Positive

GRAPH 3: OE

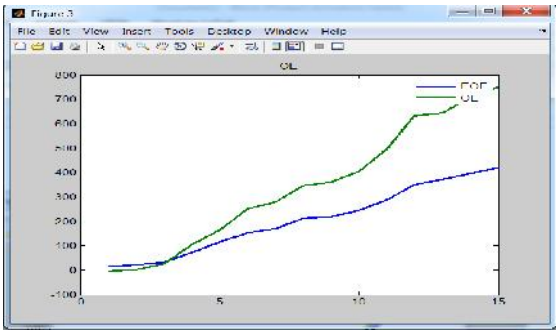

Fig 5.11 Graph on OE

GRAPH 4: PCC

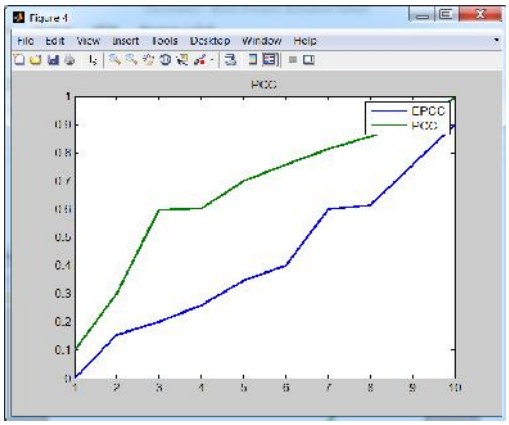

Fig 5.12 Graph on PCC

OUTPUT

Parameter	Existing	Proposed
PCC	0.91	0.9932
FP	0.96	0.89
OE	25%	13%

5.3 Performance analysis

PERFORMANCE ANALYSIS

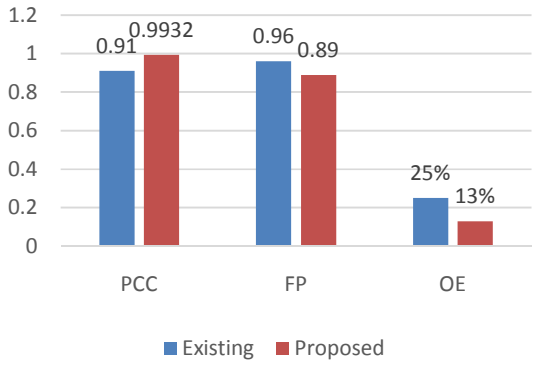

7.4 Graph of performance analysis

V. CONCLUSION

This work, an automatic change detection processing chain for rapid flood mapping is presented. Change detection based algorithms play a critical role in flood monitoring using remote sensing data, while the selection of a reference image is crucial in order to get an accurate thematic map. The Saliency-mapping is proposed to extract primary change detection information based on the log-ratio image that is generated from the reference and target image.In contrast to the traditional local-connected MRF and CRF, the FCRF considers a global view in both label and observation domains, thus enabling it to eliminate noise and to preserve detailed information at the same time.

FUTURE WORK

Future adopt a modified page rank algorithm to refine the saliency map.

It not only improves saliency detection through large salient region detection and noise tolerance in messy background,but also generates saliency maps with a well-defined object shape.

REFERENCES

1. Y. Bazi, L. Bruzzone, and F. Melgani, “An unsupervised approach based on the generalized Gaussian model to automatic change detection in multitemporal SAR images,” IEEE Trans. Geosci. Remote Sens., vol. 43, no. 4, pp. 874–887, Apr. 2005.
2. F. Bovolo and L. Bruzzone, “A split-based approach to unsupervised change detection in large-size multitemporal images: Application to tsunami-damage assessment,” IEEE Trans. Geosci. Remote Sens., vol. 45, no. 6, pp. 1658–1670, Jun. 2007.
3. T. F. Chan and L. A. Vese, “Active contours without edges,” IEEE Trans. Image Process., vol. 10, no. 2, pp. 266–277, Feb. 2001.
4. M. Chini, R. Hostache, L. Giustarini, and P. Matgen, “A hierarchical split-based approach for parametric thresholding of SAR images: Flood inundation as a test case,” IEEE Trans. Geosci. Remote Sens., vol. 55, no. 12, pp. 6975–6988, Dec. 2017.
5. J. García-Pintadoet al., “Satellite-supported flood forecasting in river networks: A real case study,” J. Hydrol., vol. 523, pp. 706–724, Apr. 2015.
6. L. Giustariniet al., “Probabilistic flood mapping using synthetic aperture radar data,” IEEE Trans. Geosci. Remote Sens., vol. 54, no. 12, pp. 6958–6969, Dec. 2016.
7. S.Grimaldi, Y.Li, V.R.N.Pauwels, and J P.Walker, “Remote sensing derived water extent and level to constrain hydraulic flood forecasting models: Opportunities and challenges,” Surv. Geophys., vol. 37, no. 5, pp. 977–1034, 2016.
8. M. Horritt, “A statistical active contour model for SAR image segmentation,”Image Vis. Comput., vol. 17, pp. 213–224, 1999.
9. J. Kittler and J. Illingworth, “Minimum error thresholding,” Pattern Recognit., vol. 19, no. 1, pp. 41–47, 1986.
10. C. H. Li and C. K. Lee, “Minimum cross entropy thresholding,” Pattern Recognit., vol. 26, no. 4, pp. 617–625, 1993.
11. S. Martinis et al., “Comparing four operational SAR-based water and flood detection approaches,” Int. J. Remote Sens., vol. 36, no. 13, pp. 3519–3543, 2015.
12. S. Martinis, J. Kersten, and A. Twele, “A fully automated TerraSAR-X based flood service,” ISPRS J. Photogramm. Remote Sens., vol. 104, pp. 203–212, Jun. 2015.

13. S. Martinis, A. Twele, and S. Voigt, "Towards operational near real-time flood detection using a split-based automatic thresholding procedure on high resolution TerraSAR-X data," Natural Hazards Earth Syst. Sci., vol. 9, no. 2, pp. 303–314, 2009.
14. D. C. Mason, L. Giustarini, J. García-Pintado, and H. L. Cloke, "Detection of flooded urban areas in high resolution synthetic aperture radar images using double scattering," Int. J. Appl. Earth Observ. Geoinf., vol. 28, pp. 150–159, 2014
15. P. Matgen, R. Hostache, G. J.-P. Schumann, L. Pfister, L. Hoffmann, and H. H. G. Savenije, "Towards an automated SAR-based flood monitoring system: Lessons learned from two case studies," Phys. Chem.Earth A/B/C, vol. 36, nos. 7–8, pp. 241–252, 2011.
16. J. Mittermayer, S. Wollstadt, P. Prats-Iraola, and R. Scheiber, "The TerraSAR-X staring spotlight mode concept," IEEE Trans. Geosci. Remote Sens., vol. 52, no. 6, pp. 3695–3706, Jun. 2014.
17. G. Moser and S. B. Serpico, "Generalized minimum-error thresholding for unsupervised change detection from SAR amplitude imagery," IEEE Trans. Geosci. Remote Sens., vol. 44, no. 10, pp. 2972–2982, Oct. 2006.
18. N. Otsu, "A threshold selection method from gray-level histograms," IEEE Trans. Syst., Man, Cybern. Syst., vol. SMC-9, no. 1, pp. 62–66, Jan. 1979.
19. L. Pulvirenti, F. S. Marzano, N. Pierdicca, S. Mori, and M. Chini, "Discrimination of water surfaces, heavy rainfall, and wet snow using COSMO-SkyMed observations of severe weather events," IEEE Trans. Geosci. Remote Sens., vol. 52, no. 2, pp. 858–869, Feb. 2014.
20. C. D. Rennóet al., "HAND, a new terrain descriptor using SRTM-DEM: Mapping terra-firme rainforest environments in Amazonia," Remote Sens. Environ., vol. 112, no. 9, pp. 3469–3481, 2008.
21. S. Schlaffer, P. Matgen, M. Hollaus, and W. Wagner, "Flood detection from multi-temporal SAR data using harmonic analysis and change detection," Int. J. Appl. Earth Observ. Geoinf., vol. 38, pp. 15–24, Jun. 2015
22. G. J.-P. Schumann, G. Di Baldassarre, and P. D. Bates, "The utility of spaceborne radar to render flood inundation maps based on multialgorithm ensembles," IEEE Trans. Geosci. Remote Sens., vol. 47, no. 8, pp. 2801–2807, Aug. 2009.
23. G. J.-P. Schumann, P. D. Bates, M. S. Horritt, P. Matgen, and F. Pappenberger, "Progress in integration of remote sensing–derived flood extent and stage data and hydraulic models," Rev. Geophys., vol. 47, no. 4, p. RG4001, 2009.
24. G. J.-P. Schumann, G. Di Baldassarre, D. Alsdorf, and P. D. Bates, "Near real-time flood wave approximation on large rivers from space: Application to the River Po, Italy," Water Resour. Res., vol. 46, no. 5, p. 8, 2010.
25. M. Sezgin and B. Sankur, "Survey over image thresholding techniques and quantitative performance evaluation," J. Electron. Imag., vol. 13, no. 1, pp. 146–168, 2004.
26. R. S. Westerhoff, M. P. H. Kleuskens, H. C. Winsemius, H. J. Huizinga, G. R. Brakenridge, and C. Bishop, "Automated global water mapping based on wide-swath orbital synthetic-aperture radar," Hydrol. Earth Syst. Sci., vol. 17, pp. 651–663, Feb. 2013.
27. J.-H. Xue and Y.-J. Zhang, "Ridler and Calvard's, Kittler and Illingworth's and Otsu's methods for image thresholding," Pattern Recognit. Lett., vol. 33, no. 6, pp. 793–797, 2012.
28. J.-H. Xue and D. M. Titterington, "Median-based image thresholding," Image Vis. Comput., vol. 29, no. 9, pp. 631–637, 2011.
29. J.-C. Yen, F.-J. Chang, and S. Chang, "A new criterion for automatic multilevelthresholding," IEEE Trans. Image Process., vol. 4, no. 3, pp. 370–378, Mar. 1995.

